

The LAMOST Spectroscopic Survey of Globular Clusters in M 31 and M 33. I. Catalog and new identifications

B.-Q. Chen^{1*}, X.-W. Liu^{1,2}, M.-S. Xiang¹, H.-B. Yuan^{2*}, Y. Huang¹, Z.-Y. Huo³, N.-C. Sun¹, C. Wang¹, J.-J. Ren^{1*}, H.-W. Zhang¹, A. Rebassa-Mansergas^{2*}, M. Yang^{4*}, Y. Zhang⁵, Y.-H. Hou⁵ and Y.-F. Wang⁵

¹ Department of Astronomy, Peking University, Beijing 100871, P. R. China; bchen@pku.edu.cn, x.liu@pku.edu.cn

² Kavli Institute for Astronomy and Astrophysics, Peking University, Beijing 100871, P. R. China

³ National Astronomical Observatories, Chinese Academy of Sciences, Beijing 100012, P. R. China

⁴ Key Laboratory of Optical Astronomy, National Astronomical Observatories, Chinese Academy of Sciences, Beijing 100012, China

⁵ Nanjing Institute of Astronomical Optics & Technology, National Astronomical Observatories, Chinese Academy of Sciences, Nanjing 210042, China

Abstract We present a catalog of 908 objects observed with the Large Sky Area Multi-Object Fiber Spectroscopic Telescope (LAMOST) in the vicinity fields of M31 and M33, targeted as globular clusters (GCs) and candidates. The targets include known GCs and candidates selected from the literature, as well as new candidates selected from the Sloan Digital Sky Survey (SDSS). Analysis shows that 356 of them are likely GCs of various degree of confidence, while the remaining ones turn out to be background galaxies and quasars, stars and H II regions in M31 or foreground Galactic stars. The 356 likely GCs include 298 bona fide GCs and 26 candidates known in the literature. Three candidates selected from the Revised Bologna Catalog of M31 GCs and candidates (RBC) and one possible cluster from Johnson et al. are confirmed to be bona fide clusters. We search for new GCs in the halo of the M31 amongst the new candidates selected from the SDSS photometry. Based on radial velocities yielded by LAMSOT spectra and visual examination of the SDSS images, we find 28 objects, 5 bona fide and 23 likely GCs. Amongst the five bona fide GCs, three have been recently discovered independently by others, the remaining 25 are our new identifications, including two bona fide ones. The new identified objects fall at projected distances ranging from 13 to 265 kpc from M31. Of the two newly discovered bona fide GCs, one is located near M33, probably a GC belonging to M33. The other bona fide GC falls on the Giant Stream with a projected distance of 78 kpc from M31. Of the 23 newly identified likely GCs, one has a projected distance of about 265 kpc from M31 and could be an intergalactic cluster.

Key words: galaxies: individual: M31, M33 - galaxies: star clusters - galaxies: Local Group

1 INTRODUCTION

Globular clusters (GCs) are excellent tracers for the studies of galaxy formation and evolution. Stars in a given GC are supposed to form almost simultaneously from gas of the same chemical composition. Their integrated colors and spectra can be relatively easily interpreted by a Simple Stellar Population (SSP; Renzini & Fusi Pecci 1988). GCs are among the intrinsically brightest objects in a galaxy, making them more easily observable than stars for a nearby galaxy. Most regular large galaxies host a large number of GCs. They are one of the oldest stellar populations known in a galaxy and thus they contain important information with regard to the earliest assemble age history of a galaxy (see Brodie & Strader 2006 for a review).

The GCs in the Andromeda galaxy M31 are of particular interest. M31 is the most luminous member of the Local Group of galaxies, as well as the nearest archetypical spiral galaxy. It serves as one of the best astrophysical laboratories for the studies of the physical and astrophysical processes that govern the morphology, kinematics and chemistry, as well as the formation and evolution of galaxies. M31 owns an abundant population of GCs, much larger than the Milky Way (MW). Barmby & Huchra (2001) estimate that M31 probably have $\sim 475 \pm 25$ GCs, about 3 times that of the MW (157 GCs; Harris 1996). This ratio of GC numbers of M31 and the MW has recently increased to more than 4 as M31 has been more thoroughly searched. In total, 638 objects are classified as confirmed GCs in the Revised Bologna Catalog of M31 GCs and candidates, Version 5 (RBC V5; Galleti et al. 2004 and most recently updated in August, 2012). More GCs and candidates are identified in recent years. di Tullio Zinn & Zinn (2014) find 7 objects, including 6 confident GCs and 1 candidate, in the M31 halo by visual examination of the Sloan digital Sky Survey (SDSS) images, excluding background galaxies based on a combination of the optical, ultraviolet, and infrared colors of the objects, as well as their photometric redshifts deduced from the SDSS data. Huxor et al. (2014) discover 59 GCs and 2 candidates in the halo of M31 again, via visual inspection of the MegaCam images of the Canada-France-Hawaii Telescope (CFHT) collected by the Pan-Andromeda Archaeological Survey (PAndAS).

At present, there are ~ 700 confirmed GCs in M31, and hundreds of candidates that need to be further checked. While many studies of GCs in M31 are based on imaging surveys (Hubble, 1932; Sargent et al., 1977; Crampton et al., 1985; Battistini et al., 1987; Kim et al., 2007; Peacock et al., 2010; Ma et al., 2015), spectroscopic observations can provide vital kinematic information and chemical composition of GCs. The first spectroscopic observations of M31 GCs was presented by van den Bergh (1969). This was followed by a large number of studies, e.g. as some of the most recent examples, Ashman & Bird (1993); Barmby et al. (2000); Perrett et al. (2002); Galleti et al. (2006); Lee et al. (2008); Caldwell et al. (2009); Veljanoski et al. (2014) and references there within. A large, systematic spectroscopic survey of GCs in M31 that covers from the disk to the outer halo, is however still lacking.

Most of the previous studies of the M31 GCs concentrate on the disk and inner halo of M31, typically within a projected distance $R_p < 30$ kpc (e.g. Crampton et al. 1985; Battistini et al. 1987; Brodie & Huchra 1991; Barmby et al. 2000; Perrett et al. 2002; Kim et al. 2007; Galleti et al. 2006; Fan et al. 2008; Caldwell et al. 2009). More recent studies have shifted their focus to the more distant GCs in the outer halo of M31, out to a projected distance of ~ 150 kpc (Galleti et al., 2007; Huxor et al., 2008; Richardson et al., 2011; Tanvir et al., 2012; di Tullio Zinn & Zinn, 2013; Mackey et al., 2013; di Tullio Zinn & Zinn, 2014; Huxor et al., 2014; Veljanoski et al., 2014; Sakari et al., 2015). A large fraction of those outer halo GCs of M31 are likely assembled via accretion of cluster-bearing satellite galaxies, as in the case of the MW (Mackey et al., 2013; Yuan, 2013; Sakari et al., 2015). These remote GCs thus serve as excellent signposts to search for the remnants and debris of tidally disrupted galaxies. Hitherto, more than 80 GCs of projected distances greater than 30 kpc have been identified, mostly by the PAndAS survey (Huxor et al. 2014 and references there within).

The Large Sky Area Multi-Object Fiber Spectroscopic Telescope (LAMOST, also named the Guoshoujing Telescope; Cui et al. 2012)¹ is a quasi-meridian reflecting Schmidt telescope with an ef-

* LAMOST Fellow.

¹ <http://www.lamost.org/website/en>

fective light-collecting aperture of about 4 m and a field of view of 5° in diameter. It is equipped with 4,000 robotic fibers and thus can record spectra of up to 4000 celestial objects simultaneously. After a two-year commissioning phase and one-year Pilot Surveys, the LAMOST Regular Surveys began in October, 2012. The large number of fibers in a wide field of view makes LAMOST an ideal facility to carry out a systematic spectroscopic survey of known GCs and candidates in M31 and M33, and, at the same, to search and identify new ones. Since the early phase of LAMOST operation, as parts of the LAMOST Spectroscopic Survey of the Galactic Anti-center (LSS-GAC; Liu et al. 2014; Yuan et al. 2015), we have use the LAMOST to carry out a systematic spectroscopic campaign of GCs and candidates in the vicinity fields of M31 and M33. In addition to GCs and candidates, other interesting objects targeted in this area include planetary nebulae (PNe) and background quasars, as well as H II regions and supergiants in M31 and M33. Some of the early results from this campaign have published, see Yuan et al. (2010) for planetary nebulae and Huo et al. (2010, 2013) for background quasars. For GCs, our purpose is two-fold – to build up a large, systematic spectroscopic dataset for GCs and candidates in this sky area, and to search for new ones. In this paper, we will present our first effort of searching for GCs in the outer halo of M31, using the LSS-GAC data accumulated hitherto. Our GC candidates are selected from the SDSS photometric data. In this paper, we will also present a catalog of all GCs and candidates targeted by LAMOST hitherto near M31 and M33. Detailed kinematic and chemical analysis of this large sample of GCs and candidates will be presented in separated papers (Chen et al. 2015, in preparation).

This paper proceeds as follows. In Section2 we describe our target selection. A brief description of the observation and data reduction is presented in Section3. In Section4 we introduce our strategy used to identify new GCs. We present and discuss the results in Section5. Finally a summary is given in Section6.

2 TARGET SELECTION

As part of the LSS-GAC, objects targeted in the M31 and M33 region include several classes of objects reachable by LAMOST at the distance of M 31 (about 770 kpc), such as GCs, PNe, H II regions and supergiants and background quasar. For a given plate, spare fibers are filled with foreground Galactic stars (Yuan et al., 2015). We hereby introduce the GC target selection of LSS-GAC. The objects are primarily selected from two sources, existing M31 GCs and candidates, and new candidates selected from the SDSS photometric catalogs. In this paper, we refer to all the targets selected from the literature as the ‘Literature sample’ and all those selected from the SDSS photometry as the ‘SDSS sample’. For all types of targets included in target input catalogs of LSS-GAC, GC targets are almost always assigned the highest priority (prior = 2).

2.1 Revised Bologna Catalog of M31 GCs and candidates

To collect all known GCs and candidates in M31, we choose RBC² (Galleti et al., 2004) as our starting point. RBC is a main repository for information of the M31 GC systems. It is a compilation of previously published catalogs. The catalog lists all the confirmed GCs (classes 1 and 8) and candidates (classes 2 and 3) at the time that the original catalog was published, and also all the objects that were originally identified as GC candidates and then subsequently recognised not to be genuine clusters, such as H II regions (class 5), background galaxies (class 4) or foreground stars (class 6). The identities of these contaminants are retained in the RBC in order to avoid their re-discoveries as M31 GCs. Before the start of each observational season (in September usually), all published newly discovered GCs in the M31 and M33 area are added to the input source catalogs of LSS-GAC for the preparation of observational plates.

² <http://www.bo.astro.it/M31/>. RBC has been updated to Version 5 since August, 2012. At the time of our target selection (2010), it was of Version 4 published in December, 2009.

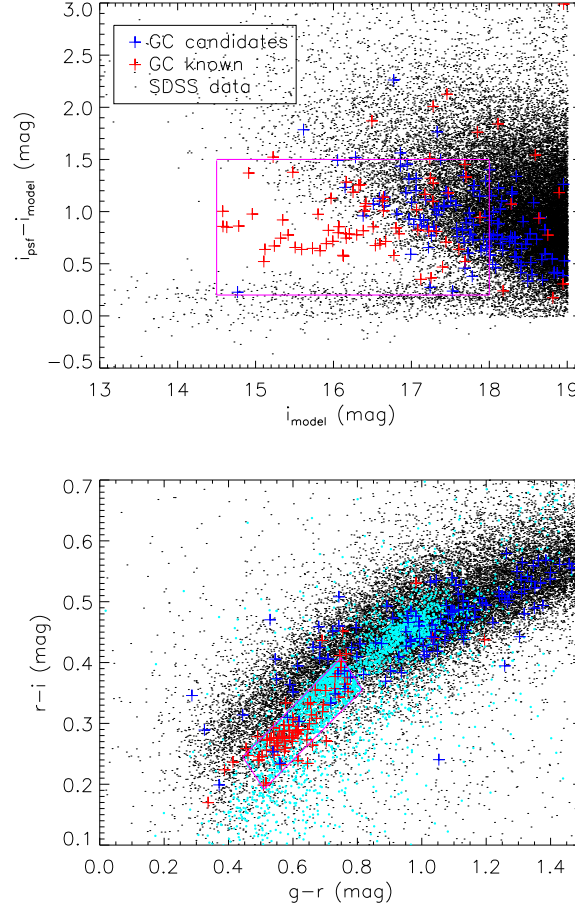


Fig. 1 *Upper panel:* Differences of i-band PSF and model magnitudes plotted against the i-band model magnitude for SDSS sources of the M31 stripes; *Lower panel:* $g - r$ versus $r - i$ color-color diagram of the same sources. In both panels, the red and blue pluses are respectively known GCs and GC candidates from Peacock et al. (2010). The pink lines delineate the area of potential candidates (see text). The cyan dots in the lower panel denote our final selected GC candidates.

2.2 New Candidates selected from the SDSS photometry

The Sloan Digital Sky Survey (SDSS; York et al. 2000) has observed a large sky area around M31. The SDSS photometric catalogs provide us the possibility of selecting interesting sources such as GC candidates in the vicinity fields of M31 and M33. Our target selections were based on the SDSS Data Release 8 (DR8; Aihara et al. 2011). The sky coverage of SDSS is incomplete around the area of M31. This unfortunately limits the extent of region of our target selections. The GC candidates are selected via the following steps.

1. The SDSS criteria for star-galaxy separation perform well, at a reliability level better than 90% up to $r = 21.6$ mag. The performance however degrades at fainter magnitudes (Abazajian et al., 2003). The absolute magnitudes M_V of GCs range between $-10.5 < M_V < -3.5$ mag (Huxor et al.,

Table 1 LAMOST observations of GC targets in the vicinity fields of M 31 and M 33.

Observational season	Observing nights	No. of Spectra	SNR(4750 Å) >5	SNR(4750 Å) >10
2011.9–2012.6	41	3292	1166	589
2012.9–2013.6	14	601	289	184
2013.9–2014.6	26	865	503	322

2008). Assuming a distance of 770 kpc for M31 (Caldwell et al., 2011), the apparent magnitudes of GCs in M31 in SDSS *i*-band range between $13.5 < i < 19.0$ mag. We discard all point sources and select GC candidates only from objects classified as non-stellar by SDSS. As GCs are red objects, the SDSS *i*-band magnitudes are used to apply an apparent magnitude cut for GC candidates. Considering the limiting magnitude of LSS-GAC survey (Yuan et al., 2015), the magnitude cut is set at $14.5 < i < 18.0$ mag.

2. The GC sample of Peacock et al. (2010) is used to help create the following GC selection criteria. The sample contains 571 confirmed GCs and 373 GC candidates. The catalog is cross-matched with the SDSS photometric catalogs for extended objects (galaxies), with a matching radius of $3''$. This yields a test sample of 83 genuine GCs and 127 GC candidates with SDSS photometry. The differences between the *i*-band point spread function (PSF) magnitudes (i_{psf}) and model magnitudes (i_{model}) are used to exclude point sources, such as the foreground stars, as well as those very extended sources, such as the background galaxies and dwarf galaxies. The upper panel of Fig. 1 plots values of $i_{\text{psf}} - i_{\text{model}}$ versus i_{model} for all SDSS non-stellar objects around the area of M31. The confirmed GCs and candidates from Peacock et al. (2010) are overplotted. Most of the confirmed GCs fall in the range $0.2 < i_{\text{psf}} - i_{\text{model}} < 1.5$ mag. This is adopted as our second selection criterion of GC candidates. Only three confirmed GCs have $i_{\text{psf}} - i_{\text{model}}$ values smaller than but close to 0.5 mag. We set the lower limit of $i_{\text{psf}} - i_{\text{model}}$ to 0.2 mag, in order to include as many GC candidates as possible.
3. GCs have relatively narrow color ranges (Peacock et al., 2010). Thus a color cut can also help to separate GCs from galaxies and stars. Only colors $g - r$ and $r - i$ are used, given the better signal-to-noise ratios (SNRs) of SDSS photometry *g*-, *r*- and *i*-bands than in *u*- and *z*-bands. A color-color diagram of all SDSS sources, the selected candidates, together with the known GCs and candidates from Peacock et al. (2010) is presented in the lower panel of Fig. 1. Most of the known GCs are located in a small area in the color-color diagram, except for a few outliers. Based on this plot, we have therefore defined the following color cuts for selecting GC candidates,

$$\begin{aligned} 0.75 < (g - r) + 1.25(r - i) < 1.26 \text{ mag} \\ -0.08 < (r - i) - 0.53(g - r) < 0.01 \text{ mag} \end{aligned}$$

In the current work, we only adopt the above color cuts to objects fainter than an *i* magnitude of 16.0 mag, considering that few background galaxies can reach an apparent *i* magnitude of brighter than 16.0 mag.

We obtain a sample of 3,585 candidates from the criteria above in the vicinity fields of M31 and M33. They are overplotted as cyan points in the bottom panel of Fig. 1. The sample is cross-matching with the existing catalogs such as RBC. Duplicates are discarded. Finally, 3,280 candidates remain. Together with GCs and candidates known in the literature, a total of more than 6,000 GC targets are included in the input catalogs of LSS-GAC. We are aware that the sample is likely to contain many contaminants, such as background galaxies and quasars. We have adopted a relatively loose set of selection criteria, taking advantage the top spectral collection rate of LAMOST.

3 OBSERVATIONS AND DATA REDUCTION

Following a two-year commissioning phase, the LAMOST Pilot Surveys were initiated in October 2011 and completed in June 2012. The Regular Surveys, expected to last five years, were initiated in October

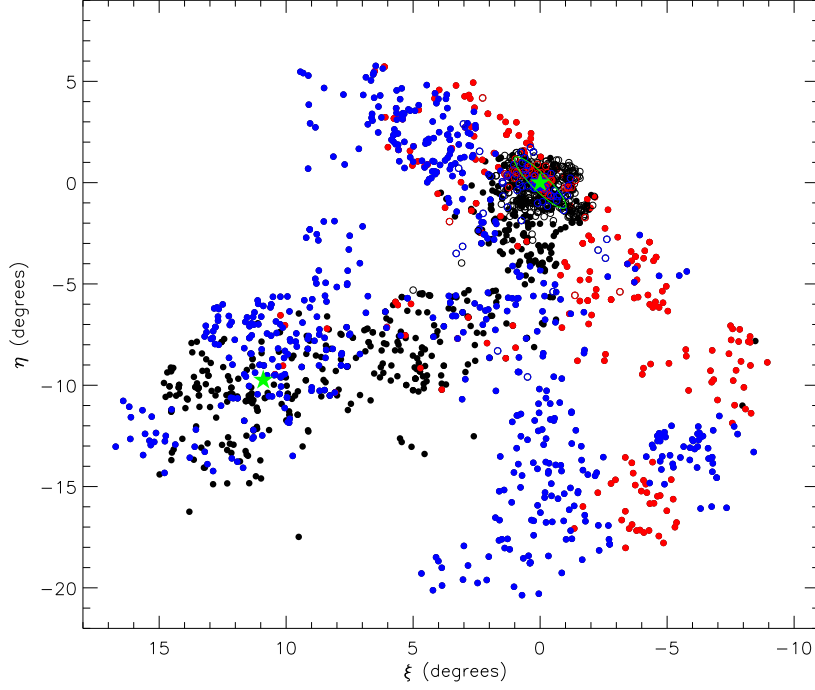


Fig. 2 Spatial distribution of GC candidates selected from the SDSS photometry (‘SDSS sample’) and targeted by LAMOST in 2011 (Black filled circles), 2012 (red filled circles) and 2013 (blue filled circles). Targets from the literature (‘Literature sample’) targeted in those three years are represented by open circles of the corresponding colors. For objects targeted multiple times, the color coding refers to the observation with the highest SNR(4750 Å). The green stars mark the central positions of M31 and M33, respectively. The green ellipse represents the optical disk of M31 of radius $R_{25} = 95'.3$.

2012. In the current work we present results based on data collected by LAMOST in the 2011, 2012 and 2013 observational seasons, i.e. from the Pilot Survey and the first two years of the Regular Surveys.

Being a quasi-meridian reflecting Schmidt telescope, LAMOST only observes a given field of plate between 2 h before and after the transit. The M31 and M33 area ($0 < \text{RA} < 30^\circ$, $25 < \text{Dec.} < 50^\circ$) are targeted by LAMOST from September to January of the next year in a given observational season, which starts in September and ends in June of the following year. The plates are observed in nights of dark or grey lunar conditions. Typically 2–3 exposures are obtained for each plate, with an integration time per exposure varying, depending on the weather conditions, between 600–1200 s, 1200–1800 s and 1800–2400 s for bright (B), median (M) and faint (F) plates, respectively. Some observing nights reserved to monitor the telescope performance are also used to observe M31 and M33 plates. For most plates, the seeing varies between 3 – 4 arcsec, with a typical value of about 3.5 arcsec (Yuan et al., 2015).

LAMOST has a field of view (FoV) of 5° in diameter. There are 16 low-resolution spectrographs, each accommodating 250 auto-positioning fibers. The parking positions of fibers evenly distributed in the focal plane, except for a few regions reserved for guiding cameras and the central Shack-Hartmann sensor. Each fiber has a diameter of 3.3 arcsec projected on the sky. LAMOST is implemented with slit masks of width $2/3$ the fiber diameter, i.e. 2.2 arcsec, yielding a spectral resolving power of about $R \sim 1800$. The spectra cover a wavelength range of 3700–9000 Å. The light entering each spectrograph

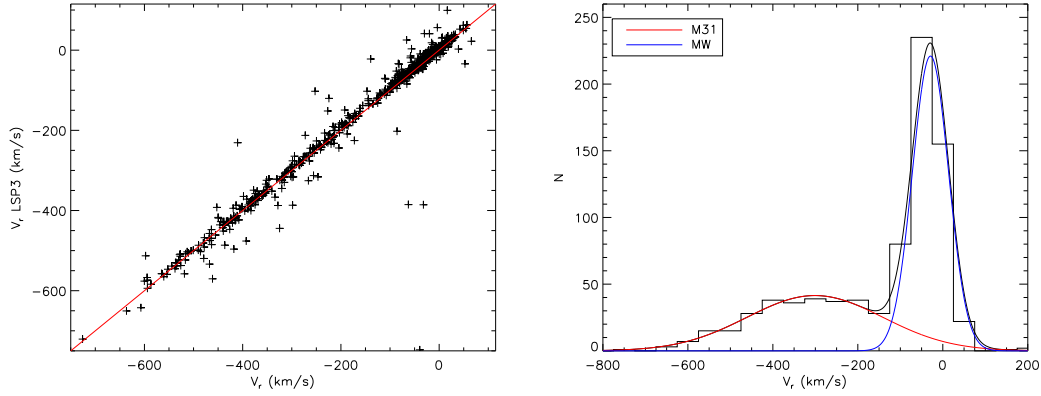


Fig. 3 *Left panel:* Radial velocities derived in the current work for all non-galaxy candidates that have $\text{SNR}(4750 \text{ \AA}) > 5$ per pixel, compared to the values yielded by the LSP3 (Xiang et al., 2015b). A red line denoting complete equality is overplotted to guide the eyes. *Right panel:* Histogram distribution of newly derived radial velocities for the same set of objects. The means and standard deviations of Gaussians overplotted are taken from Galleti et al. (2006).

is dispersed and recorded in two arms, covering $3700 - 5900 \text{ \AA}$ and $5700 - 9000 \text{ \AA}$ in the blue and in the red, respectively. In each arm of a given spectrograph, a 4096×4096 CCD, with a squared pixel size of $12 \mu\text{m}$, is used to record the light signal (Cui et al., 2012). One CCD pixel corresponds to about 0.56 \AA and 0.82 \AA in the blue and in the red, respectively.

We give a summary of the observations of GC targets observed by LAMOST in the M31 and M33 area in Table 1. By June 2014, a total of 131 plates with GC targets have been collected, yielding 4,758 spectra of 1,991 unique GC. Most of the spectra (3292) were observed in the 2011 observational season, while 601 and 865 spectra were collected in the 2012 and 2013 seasons, respectively. About 42.2, 25.1, 12.0, 7.9, 4.9, 4.0 and 2.3 per cent objects were targeted by 1 to 7 times, respectively. There are 1958, 1095 and 465 spectra having $\text{SNR}(4750 \text{ \AA})$ greater than 5, 10 and 20 per pixel, respectively. As GCs are red objects, the SNRs are better in the red than in the blue. This is reflected in the fact that there are 3101, 2398 and 1488 spectra that have $\text{SNR}(7450 \text{ \AA})$ greater than 5, 10 and 20 per pixel, respectively.

Fig.2 plots the spatial distribution in the $\xi - \eta$ plane of all GC targets observed by LAMOST by June 2014 in the vicinity fields of M31 and M33 (located at $\xi = 11^\circ.3$, $\eta = -10^\circ.1$ on this map). Here ξ and η are respectively the offsets in Right Ascension and Declination relative to the optical center of M31 (RA= $00^{\text{h}}42^{\text{m}}44.30^{\text{s}}$; Dec= $+41^\circ16'09.0''$; from Huchra et al. 1991; Perrett et al. 2002). The green ellipse in Fig.2 represents the optical disk of M31, with an optical radius $R_{25} = 95'.3$ (de Vaucouleurs et al., 1991), an inclination angle $i = 77^\circ$ and a position angle P.A. = 38° (Kent, 1989). Candidates of the SDSS Sample are mostly located in the outer halos of M31 and M33, while those of the Literature Sample fall mostly near the disk and inner halo of M31.

All the spectra were first processed with the LAMOST 2-D pipeline (Version 2.6, Luo A.-L., et al. 2015), including steps of bias subtraction, cosmic-ray removal, 1D spectral extraction, flat-fielding, wavelength calibration, and sky subtraction. The blue- and red-arm spectra are processed separately in the 2D pipeline and then joined together after flux calibration, which is carried out using a pipeline specifically designed for the LSS-GAC survey (Xiang et al., 2015a). No scaling or shifting is performed in cases where the blue- and red-arm spectra are not at the same flux level in the overlapping region, as it is unclear whether the misalignment is caused by poor flat-fielding or sky subtraction, or both. Note that in the current implementation of flux-calibration of Xiang et al. (2015a), the telluric absorp-

tions, including the prominent Fraunhofer A band at 7590 \AA and B band at 6867 \AA have not been removed. Finally, for objects that have been observed for multiple times in different plates, spectra of lower SNR(4750 \AA) are scaled by low order polynomials to match continuum level of the spectrum of highest SNR(4750 \AA) and then combined all together, with each spectrum weighted by the inverse square of errors.

For stars observed in the LSS-GAC, stellar parameters deduced from the spectra with the LAMOST Stellar Parameter Pipeline (LASP, Luo A.-L., et al. 2015), including radial velocities and basic stellar atmospheric parameters (T_{eff} , $\log g$ and $[\text{Fe}/\text{H}]$), are available from the LAMOST DR1 (Luo A.-L., et al., 2015). A separate pipeline, the LAMOST Stellar Parameter Pipeline at Peking University (LSP3; Xiang et al. 2015b), has been developed at Peking University to determine the radial velocities and values of T_{eff} , $\log g$ and $[\text{Fe}/\text{H}]$. The LSP3 determines the stellar atmospheric parameters by spectral template matching with the MILES empirical spectral library (Sánchez-Blázquez et al., 2006; Falcón-Barroso et al., 2011), instead of the ELODIE library (Prugniel & Soubiran, 2001; Prugniel et al., 2007) used by the LAMOST default pipeline. The LSP3 is applied to all spectra having a SNR(4750 \AA) > 2.76 per pixel, including GC targets of interest here. The LSP3 however treats the GC spectra as of stars.

For our GC targets, we have thus derived their radial velocities, as well as the ages and metallicities by comparing the observed spectra with those of SSP models (Chen et al. 2015, in prep.), using the public code ULYSS³ (University of Lyon Spectroscopic analysis Software; Koleva et al. 2009). ULYSS is an open-source software package used to study the stellar populations of galaxies star clusters, as well as to derive the atmospheric parameters of stars. It performs spectral fitting with a linear combination of non-linear components, convolved with a line-of-sight velocity distribution and multiplied by a polynomial continuum. For likely GC candidates in our sample, we use the routines to fit the spectra and determine the target properties. SSP models computed with the MILES library (Vazdekis et al., 2010) are adopted. The MILES spectra cover the wavelength range $3540\text{--}7400 \text{ \AA}$ at a resolution of 2.5 \AA FWHM . Only spectra having a SNR(4750 \AA) > 5 or SNR(7450 \AA) > 10 per pixel are analyzed. Spectra that have a large number of bad pixels ($> 1/3$ of the total) are also excluded. This leaves us with 908 unique objects in our sample. The radial velocities are derived if they fall in the range $-2000 < V_r < 2000 \text{ km s}^{-1}$. Background galaxies, typically having a radial velocity $V_r > 5000 \text{ km s}^{-1}$, are first excluded by visually examination before fitting the observed spectra with models.

By internal tests using multiple observations of duplicate objects and external tests using common targets with previous studies in the literature, we conclude that for GC targets with SNR(4750 \AA) > 5 , the derived radial velocities have achieved an accuracy of better than 12 km s^{-1} (Chen et al. 2015, in prep.). In the left panel of Fig. 3, we compare our newly derived radial velocities with those delivered by the LSP3 (Xiang et al., 2015b) for all the non-galaxy objects that have SNR(4750 \AA) > 5 . They are in very good agreement, with a marginal system offset and scatter of $V_r - V_{r,\text{LSP3}} = -5 \pm 6 \text{ km s}^{-1}$. A histogram distribution of the newly derived radial velocities for the same set of objects is presented in the right panel of Fig. 3. A double two Gaussian distribution, with one peak at around -30 km s^{-1} representing the MW foreground stars, and another around -300 km s^{-1} for M31 objects, is clearly visible. Also overplotted are two Gaussians, with the parameters taken from Galleti et al. (2006). The first Gaussian has a mean $\mu = -301.0 \text{ km s}^{-1}$ and a standard deviation $\sigma = 160.0 \text{ km s}^{-1}$ for the M31 GCs, and the second one has a mean $\mu = -29.0 \text{ km s}^{-1}$ and a standard deviation $\sigma = 42.6 \text{ km s}^{-1}$ for the MW foreground stars. The sum of the two Gaussian functions fit nicely the velocity distribution. The Figure shows that there is a large number of foreground MW stars contaminating the sample.

4 THE GC IDENTIFYING

Some of our targets that are clearly not GCs objects can be readily singled out based on the spectra obtained. There are 15 objects in our sample whose spectra display strong TiO bands typical of M-type

³ <http://ulyss.univ-lyon1.fr/>

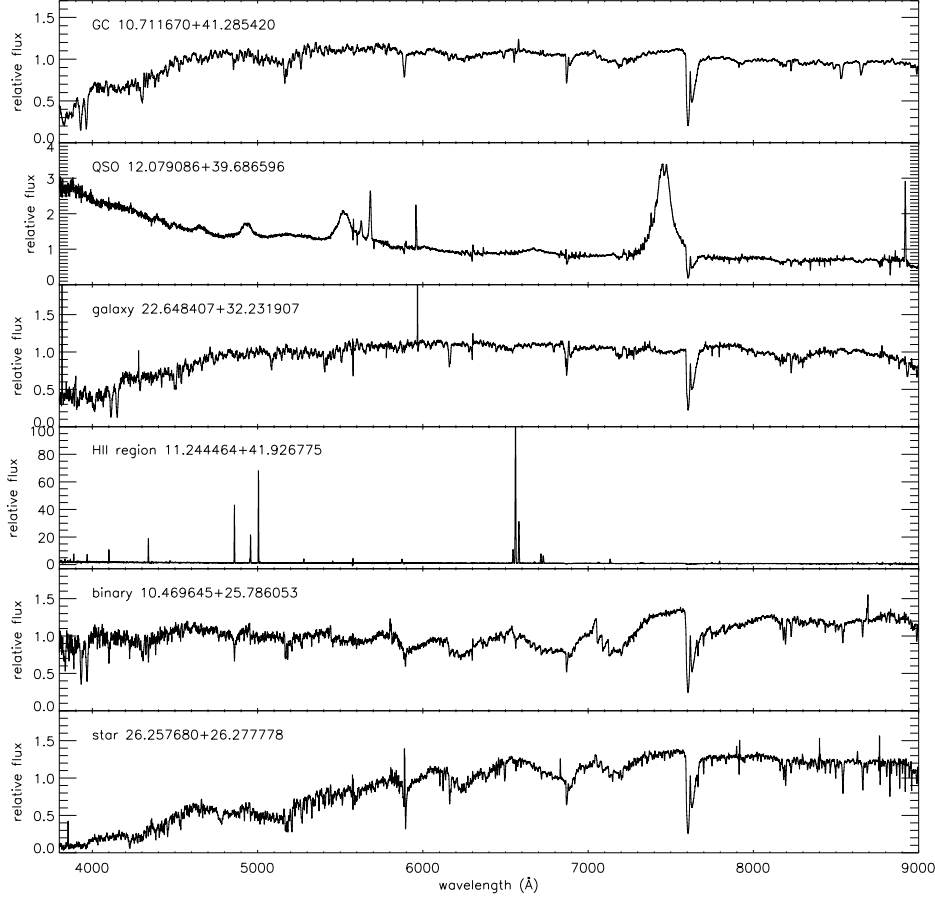


Fig. 4 Example LAMOST spectra of targets classified as non-GC objects, as well as that of a known GC. From top to bottom, the Figure plots, respectively, the LAMOST spectra of a known GC, a quasar, a galaxy, an H II region, a white-dwarf-main-sequence binary and an M-type main-sequence star. For each spectrum, the object type and coordinates (RA and Dec. in degree) are labelled.

stars. One target shows a composite spectrum, a blue component of a white dwarf and a red component of an M dwarf, i.e. this is a white-dwarf-main-sequence binary. These targets will be classified as stars in our catalog. There are 8 objects displaying strong and broad emission lines characteristic of quasars, and are classified as quasars. Example spectra of those classified as non-GC objects are presented in Fig. 4.

In addition to the aforementioned contaminants of special spectral characterises, there are two other main groups of contaminants. One is the background galaxies and the other the foreground Galactic stars. With the information of radial velocities, we can easily identify the background galaxies since they generally have very large positive radial velocities, in contrast to negative velocities of a mean around -301 km s^{-1} and a dispersion about 160 km s^{-1} (Galleti et al. 2006; see also the right panel of Fig. 3) for GCs of M31. Amongst our SDSS Sample targets, we find 218 background galaxies.

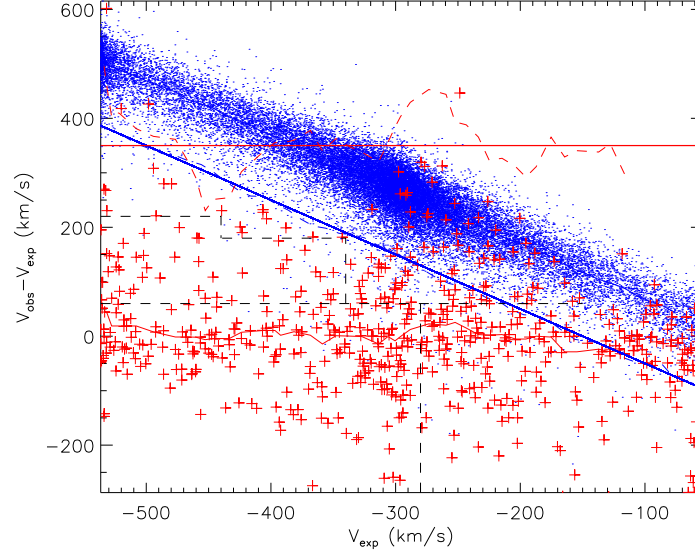


Fig. 5 Comparison of the observed and expected radial velocities of known GCs from the literature (red pluses) and of foreground MW stars simulated with the Besançon model (blue dots). Here we plot the differences between the observed and expected radial velocities against the expected radial velocities. The blue and red solid lines give the binned median values for known M31 GCs and the simulated foreground stars, respectively, with the 3σ scatters delineated by the blue and red dashed lines, respectively. The blue solid straight line marks a line of constant $V_r = -150 \text{ km s}^{-1}$, while the red solid straight line traces a line of $V_r - V_{\text{exp}} = 350 \text{ km s}^{-1}$.

Identifying foreground MW stars is more difficult. For this purpose, the information of radial velocities is first used. For a disk galaxy such as M31, the radial velocity V_r can be approximated by $V_r = V_0 + V(R) \sin\xi \cos\theta$ (Rubin & Ford, 1970), where V_0 is the systemic radial velocity, ξ is the angle between the line of sight and the norm of the galaxy disk plane, $V(R)$ is the rotational velocity in the plane at a radius R . $\cos\theta = X/R$, where X is the position along the major axis. If we assume the rotation curve has a constant velocity, $V(R) = \text{const.}$, then there is a linear relation between V_r and object position. Drout et al. (2009) present a relation to calculate the expected radial velocity V_{exp} , based on a least-squares linear regression to the radial velocity measurements of H II regions in M31,

$$V_{\text{exp}} = 295 + 241.5(X/R) \text{ km s}^{-1}. \quad (1)$$

We collect known GCs in M31 that have radial velocities measured in the literature: RBC V5 (Galleti et al., 2006, and references there within), Caldwell et al. (2009) and Veljanoski et al. (2014). Radial velocities of 663 known M31 GCs are collected. These GCs cover a wide spatial distribution, with positions along the major axis spanning $-85 < X < 102 \text{ kpc}$ and along the minor axis ranging $-118 < Y < 122 \text{ kpc}$. The linear relation between X/R and V_{exp} given by Eq. (1) works well for these known GCs.

For the foreground Galactic stars, the Besançon model (Robin et al., 2003) is used to simulate the velocity distribution of Galactic stars in a $5 \times 5 \text{ sq. deg.}$ region around M31. We plot the differences between the observed radial velocities of all the known M31 GCs and the expected velocities given by Eq. (1) in Fig. 5. Also overplotted are the differences between the modelled radial velocities of foreground Galactic stars and those given by Eq. (1). All the M31 GCs fall along the line of zero differences

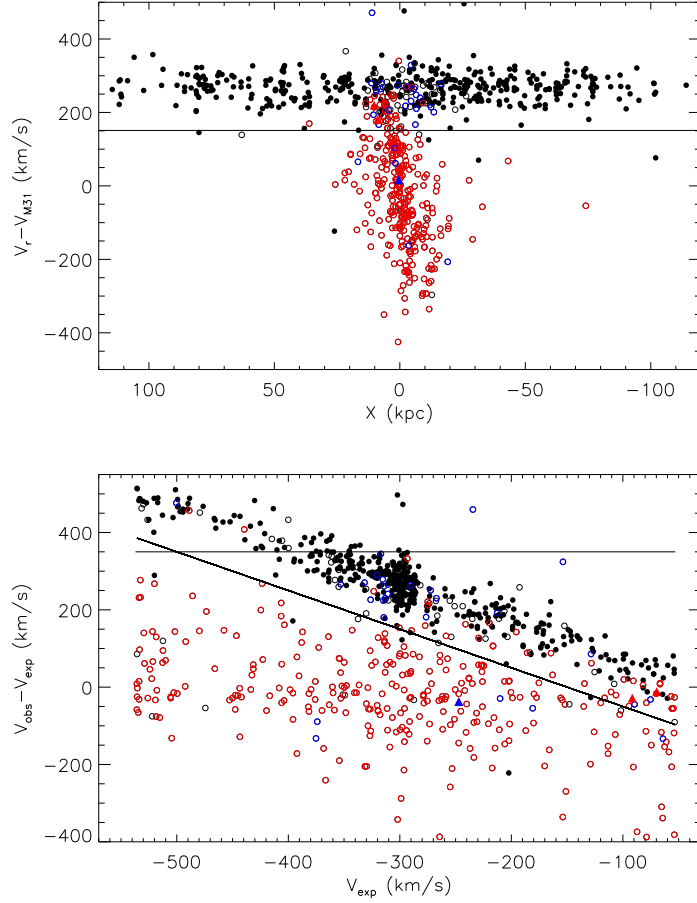


Fig. 6 *Upper panel:* Velocity offsets relative to the systematic value of M 31, plotted against major-axis distance X , for GCs and GC candidates observed by LAMOST. *Lower panel:* Same as Fig. 5 but for GCs and GC candidates observed by LAMOST. In both panels the filled circles, open circles and filled triangles represent targets from the SDSS Sample, and those from RBC and from Johnson et al. (2012), respectively. For the RBC targets, known GCs (classes 1 and 8) are marked in red, GC candidates (class 2) in blue and objects of other classes in black. For the Johnson et al. (2012) targets, confirmed clusters (flagged by a ‘c’) are marked in red and possible clusters (flagged by a ‘p’) in blue.

($V_r - V_{\text{exp}} \sim 0 \text{ km s}^{-1}$), while all the simulated foreground Galactic stars locate along a line of radial velocity $V_r \sim 0 \text{ km s}^{-1}$. Lines delineating 3σ scatters of velocity differences for both M31 GCs and simulated Galactic stars are also plotted in Fig. 5. Essentially all the Galactic stars fall above the straight line of $V_r = -150 \text{ km s}^{-1}$, except for a few (< 2 per cent) that have a radial velocity less than -150 km s^{-1} . Candidates in our sample that have a radial velocity $V_r < -150 \text{ km s}^{-1}$ thus have a high probability of being genuine GCs in M31. The same criterion is used by Galleti et al. (2006) to classify bona fide GCs. Also overplotted in Fig. 5 is the criterion adopted by Drout et al. (2009) to select M31 stars from the Galactic foreground stars. The two criteria are almost identical. Only five (1 per cent) M31 GCs fall above the line of $V_r - V_{\text{exp}} > 350 \text{ km s}^{-1}$ in Fig. 5, approximately the 3σ upper limit for the known

M31 GCs. We classify all candidates in our sample that have a radial velocity $V_r - V_{\text{exp}} > 350 \text{ km s}^{-1}$ as foreground Galactic stars. For sample targets of $V_r > 150.0 \text{ km s}^{-1}$ but $V_r - V_{\text{exp}} < 350 \text{ km s}^{-1}$, the probabilities of the targets being foreground Galactic stars cannot be neglected. These objects are therefore classified as possible GC candidates in the current work.

The above criteria for classifying candidates are then applied to all targets in our sample, excluding those that have been classified as background quasars, galaxies or objects of special spectral characteristics, as described above. We calculate the differences $V_r - V_{\text{exp}}$ for the remaining objects in our sample and plot the differences against V_{exp} in Fig.6. The boundaries separating highly confident GC candidates, possible GC candidates and stars are also overplotted. The classification leads us a list of 5 new M31 GC candidates and 352 possible candidates from the SDSS Sample, in addition to those from the Literature Sample.

A method similar to that used by di Tullio Zinn & Zinn (2013) is then applied to search for genuine GCs amongst the 5 candidates and 352 possible candidates from the SDSS Sample of targets. We visually examine the SDSS images to search for morphological evidence of clusters, using the cutout images retrieved from the SDSS website⁴. Some objects are found to be clearly not clusters and are most likely binaries, stars or background galaxy pairs. For some objects, the SDSS r -band images were retrieved for a more detailed inspection. We adopt the classification scheme of di Tullio Zinn & Zinn (2013). The objects are classified as GCs and candidates by the same criteria as category 1 for GCs and categories 2 and 3 for candidate clusters, respectively. A large number of the candidates cannot be reliably classified given the relatively poor resolution of SDSS images. They are denoted as unknown objects in our catalog. Finally, we are left with 5 GCs, 23 candidate clusters and 277 unknown objects.

Using the criteria described above, for the original 553 GC targets selected from the SDSS photometry, we are left with

1. 5 M31 GCs of $V_r < 150.0 \text{ km s}^{-1}$ or $V_r > 150.0 \text{ km s}^{-1}$ but $V_r - V_{\text{exp}} < 350 \text{ km s}^{-1}$, with supporting morphological evidence;
2. 23 M31 GC candidates of $V_r > 150.0 \text{ km s}^{-1}$ but $V_r - V_{\text{exp}} < 350 \text{ km s}^{-1}$, with supporting morphological evidence;
3. 218 background galaxies of large radial velocities;
4. 22 stars of $V_r - V_{\text{exp}} > 350 \text{ km s}^{-1}$, with supporting morphological evidence or spectra information of being stars;
5. 8 quasars with strong broad emission lines;
6. 277 unknown objects of $V_r > 150.0 \text{ km s}^{-1}$ but $V_r - V_{\text{exp}} < 350 \text{ km s}^{-1}$, with no clear morphological evidence and spectra information for a proper classification.

5 RESULT AND DISCUSSION

5.1 Newly discovered GCs in the halo of M31

The positions and radial velocities of the resulted 5 GCs from the SDSS Sample are listed in Table 2. Two are new discoveries, the other three are recently discovered independently by di Tullio Zinn & Zinn (2014, LAMOST-4) and Huxor et al. (2014, LAMOST-3 and 5). LAMOST-3 and LAMOST-5 have been spectroscopically observed recently by Veljanoski et al. (2014). The radial velocities derived by Veljanoski et al. (2014) are consistent with our measurements. For LAMOST-1, 2 and 4, no spectroscopic observations have been published yet. Also listed in Table 2 are their SDSS colors and magnitudes, $g - r$, $r - i$ and i , based on the model magnitudes yielded by the SDSS photometric pipeline. The differences between the i -band PSF and model magnitudes for all objects are also listed in the Table. From values of the foreground extinction as given by the extinction map of Schlafly et al. (2014) for the M31 and M33 vicinity fields, and a distance of 770 kpc to M31 as given by Caldwell et al. (2011), we estimate the absolute V -band magnitude of these objects⁵. With $M_V < -6 \text{ mag}$, they appear to be

⁴ <http://skyserver.sdss.org/dr12/en/tools/chart/listinfo.aspx>

⁵ For photometric transformation, we use the relation of Lupton & Ivezić (2005), $V = g - 0.5784(g - r) - 0.0038 \text{ mag}$.

Table 2 Positions and properties of 5 confirmed GCs from the SDSS Sample of targets.

Name	RA (deg)	Dec. (deg)	X (kpc)	Y (kpc)	R_p (kpc)	$g - r$ (mag)	$r - i$ (mag)	i_{model} (mag)	M_V (mag)	$i_{psf} - i_{model}$ (mag)	V_r (km s ⁻¹)
LAMOST-1	12.23263	35.56682	-49.75	-60.34	78.21	0.77	0.39	17.85	-6.19	1.28	-55
LAMOST-2	24.07521	30.27437	-11.51	-204.43	204.75	0.71	0.33	17.80	-6.18	0.49	-175
LAMOST-3 ^a	11.18990	43.44303	26.06	14.11	29.63	0.58	0.28	16.97	-7.05	1.09	-424
LAMOST-4 ^b	9.03580	39.29165	-31.37	-2.75	31.49	0.56	0.26	17.12	-6.89	1.18	-230
LAMOST-5 ^c	14.73496	42.46061	38.06	-21.18	43.56	0.55	0.27	15.54	-8.44	1.04	-144

^a Identified previously by Huxor et al. (2014) as ‘PAndAS-36’ in their Table 1.

^b Identified previously by di Tullio Zinn & Zinn (2014) as ‘D’ in their Table 1.

^c Identified previously by Huxor et al. (2014) as ‘PAndAS-46’ in their Table 1.

brighter than the average of M31 GCs, which is probably caused by the relatively bright magnitude limit adopted by us when selecting the SDSS Sample of GC candidates.

The LAMOST spectra of the five GCs are plotted in Fig. 7. Only the spectral range, 4000–5400 Å, used to calculate the radial velocities is shown (Chen et al., in prep.). Also overplotted are the best-fit SSP model spectra. Most spectra have a good SNR and the model spectra fit the observations nicely. The spectrum of LAMOST-4 has a relatively low SNR, yet the correlation between the observed and model spectra remains to be good. The spectra differ from object to object, indicating their different properties. However, they all have a relatively weaker Mg I (5176.7 Å) feature, suggesting that they are all very old GCs. GCs of lower metallicities generally have stronger Balmer lines (Vazdekis et al., 2010). Based on this, it seems that LAMOST-5 is a very metal-poor GC, while LAMOST-1 is metal rich. Fig. 8 displays the SDSS r -band images of the five objects. They all exhibit morphological appearance unambiguous for typical M31 GCs.

Table 3 lists the 23 newly discovered candidate clusters from the SDSS Sample. They all have radial velocities and spectral types compatible with being M31 GCs. Their morphologies also look like M31 GCs rather than stars or galaxies. Unfortunately, the SDSS image quality of those objects are not good enough to make a firm conclusion. To confirm whether they are GCs, images of better resolution are preferred. The radial velocities of these new GC candidates range between -224 and 8 km s⁻¹. In Table 3 we also list their metallicities yielded by the LSP3 (Xiang et al., 2015b) for reference. Note that the LSP3 treats all objects as stars. If these objects are indeed stars, then the LSP3 results show that most of them are relatively metal-rich, with a metallicity $[Fe/H] \sim 0$ dex, suggesting that they are unlikely to be foreground MW halo stars. This is another indirect indication that they are probably M31 GCs. Some of them are quite extended, such as LAMOST-C14, C17 and C23. Thus it is possible that some of them could be ultra-compact dwarf galaxies.

In Fig. 9 we present the radial velocity and spatial distributions of these newly confirmed M31 GCs and candidates. In the upper panel, previously known GCs from RBC (Galleti et al., 2006), Caldwell et al. (2009) and Veljanoski et al. (2014) are also overplotted, along the H I rotation curve from Carignan et al. (2006). The new objects spread over a wide area around M31 and M33, especially south of M31, where by definition, X , the projected distance along the major axis of M31 is negative, $X < 0$ kpc. Two candidates, LAMOST-C15 and LAMOST-C21, have a projected distance X close to -150 kpc. Six objects fall at relatively small projected distances to the center of M31, $13 < R_p < 30$ kpc. They fit much better the rotation curve than the more remote ones of $R_p > 30$ kpc. Most of the new remote GCs and candidates at large projected distances show almost no correlation with the M31 rotation, as for those known M31 halo GCs, suggesting that they are possibly accreted ones. The newly confirmed GC, LAMOST-1, falls on the Giant Stream and LAMOST-4 on G1 Clump. Two candidates, LAMOST-C13 and C23 locate in the Eastern Cloud. LAMOST-7 and C11 lie in the North-East Structure, while LAMOST-C10 and C14 in Stream D. Interestingly, LAMOST-C14 appears look like an ultra-compact dwarf galaxy morphologically, possibly the remnant of an accreted and tidally disrupted dwarf galaxy.

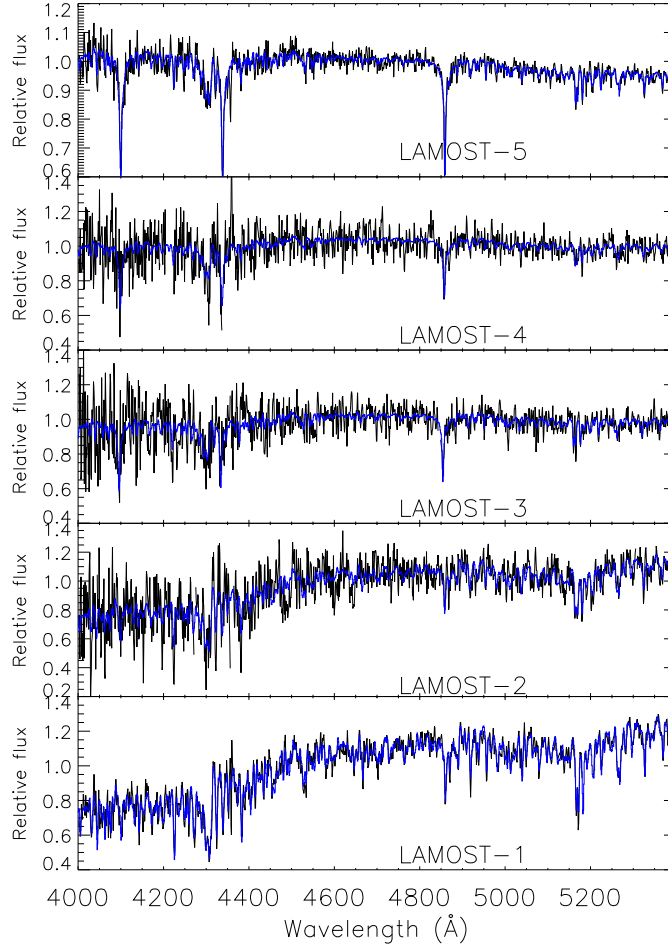


Fig. 7 LAMOST spectra of the 5 objects listed in Table 2. The observed and best-model spectra are plotted in black and blue, respectively. The plots are labelled with the LAMOST names of the objects.

These objects thus provide good opportunity study the assemblage history of M31 halo (Chen et al. in prep.).

LAMOST-2 falls in the halo region of M33 (see the lower panel of Fig. 9), together with 6 GC candidates. These objects have radial velocities ranging from -175 to 0 km s^{-1} , close to the M33 system radial velocity of -179.2 km s^{-1} (McConnachie, 2012). In particular, LAMOST-2, the GC closest to M33, has a radial velocity of -175 km s^{-1} . They could thus be GCs belonging to M33. LAMOST-1 is the most distant confirmed GC from M31 in our sample, except for those possibly belonging to M33. It has a projected distance from M31 of $R_p = 78 \text{ kpc}$. LAMOST-C15, C17 and C21 have very large distances from both M31 and M33. They are possibly intergalactic GCs.

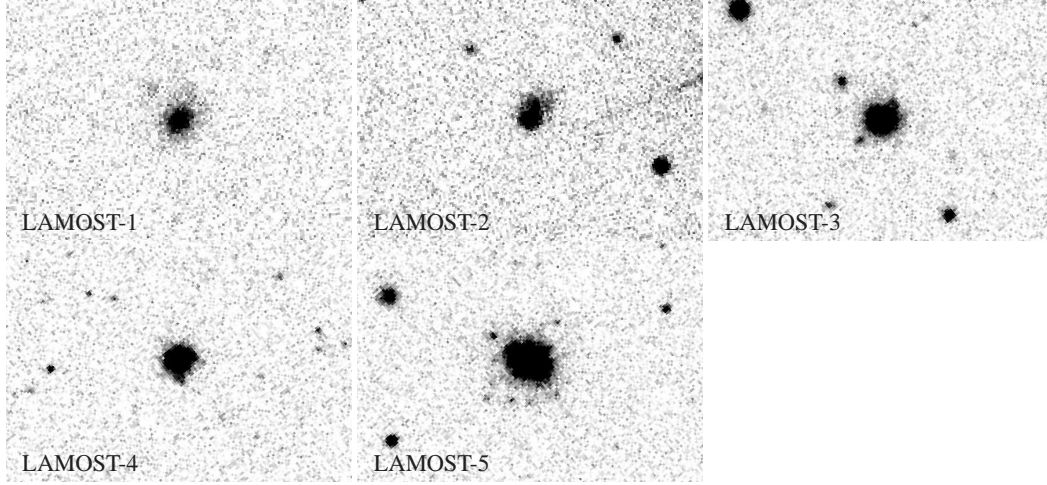


Fig. 8 Thumbnails of SDSS r -band images of the five objects listed in Table 2. The object names are labelled. Each thumbnail is about $1' \times 0.7'$ in size, with north at the top and east to the left.

Table 3 Positions and properties of newly discovered GC candidates.

Name	RA (deg)	Dec. (deg)	X (kpc)	Y (kpc)	R_p (kpc)	$g - r$ (mag)	$r - i$ (mag)	i_{model} (mag)	$i_{psf} - i_{model}$ (mag)	V_r (km s $^{-1}$)	[Fe/H] ^a (dex)
LAMOST-C01	8.60064	32.95713	-101.96	-49.84	113.49	1.09	0.45	15.56	0.23	-224	-0.0
LAMOST-C02	17.44993	44.90916	80.05	-18.98	82.27	0.34	0.06	15.36	0.30	-155	-0.9
LAMOST-C03	12.31295	41.51334	12.79	-10.80	16.74	0.88	0.34	15.51	0.21	-12	-0.1
LAMOST-C04	22.98796	30.96388	-14.04	-189.52	190.04	1.26	0.47	14.92	0.26	-51	-0.0
LAMOST-C05	20.15258	36.50384	16.66	-116.19	117.38	0.67	0.29	17.85	0.63	-60	-1.9
LAMOST-C06	9.77655	41.91114	1.24	12.50	12.56	1.24	0.52	15.54	0.24	-28	0.1
LAMOST-C07	10.13945	42.48282	9.54	14.31	17.20	0.54	0.17	14.52	0.25	-23	0.2
LAMOST-C08	11.51354	42.71485	20.38	5.53	21.12	0.66	0.08	14.62	0.30	-8	-0.2
LAMOST-C09	11.56175	42.85695	22.17	6.35	23.06	0.52	0.31	14.83	0.33	-26	-0.2
LAMOST-C10	14.79318	43.93129	53.38	-8.71	54.09	0.76	0.30	15.12	0.27	-26	-0.7
LAMOST-C11	15.96447	45.29663	74.50	-5.05	74.67	0.59	0.21	15.62	0.22	-39	-0.2
LAMOST-C12	23.75001	32.17213	3.55	-184.21	184.24	0.71	0.32	16.97	0.47	-33	-1.3
LAMOST-C13	20.41774	42.53701	76.72	-61.78	98.51	0.90	0.18	14.09	0.24	-42	-0.4
LAMOST-C14	16.00398	40.59559	27.55	-47.26	54.71	0.96	0.40	15.15	1.28	-61	-1.3
LAMOST-C15	11.48103	26.65204	-147.20	-127.14	194.51	0.42	0.37	14.18	0.22	-49	-0.3
LAMOST-C16	25.11528	30.62788	0.48	-209.17	209.17	0.90	0.45	15.34	1.43	0	-0.2
LAMOST-C17	25.05346	25.09957	-51.10	-259.52	264.50	0.94	0.51	15.79	1.44	8	0.0
LAMOST-C18	23.84216	29.55245	-20.21	-209.28	210.25	0.90	0.43	15.70	1.29	-11	-0.1
LAMOST-C19	26.13748	30.74861	10.20	-215.79	216.03	0.87	0.47	15.88	1.36	-85	-0.1
LAMOST-C20	26.02594	30.52029	7.16	-217.11	217.22	0.95	0.43	15.27	1.38	-94	-0.2
LAMOST-C21	12.47521	25.83369	-147.98	-143.10	205.86	0.65	0.33	15.32	1.09	-50	-1.8
LAMOST-C22	11.73863	29.69350	-114.12	-104.78	154.92	1.08	0.48	15.89	1.38	-26	-0.7
LAMOST-C23	21.04854	41.70561	73.17	-74.07	104.12	0.91	0.47	15.66	1.40	-59	-1.5

^a Metallicities yielded by the LSP3 which assumes all objects as stars (Xiang et al., 2015b).

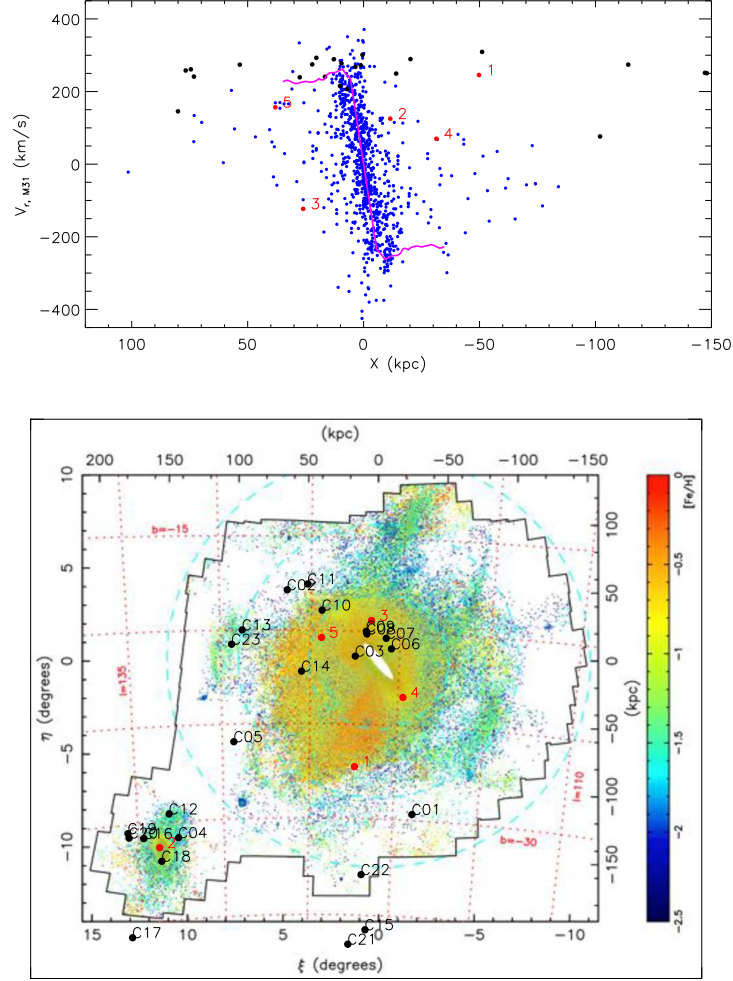


Fig. 9 *Upper panel:* Radial velocities plotted against the major axis distances for previously confirmed M31 GCs (blue dots), newly identified GC candidates (black dots) and genuine GCs (red dots). The pink line is the H I rotation curve from Carignan et al. (2006). $V_{r,M31}$ is the line-of-sight velocity in the Andromeda-centric reference system. *Lower panel:* Spatial distribution of newly identified GCs and candidates, overplotted on a stellar metallicity map from the PAndAS survey (Ibata et al., 2014). Red and black dots represent bona fide GCs and candidates, respectively.

5.2 Updates to the Literature Sample

Except for candidates from the SDSS Sample, there are 355 known clusters and candidates from the Literature Sample. They mostly fall near the disk of M31, within a projected distance $R_p < 30$ kpc. Most of the sources are from the RBC. A couple of objects are recent discoveries from the Panchromatic Hubble Andromeda Treasury (PHAT) survey (Johnson et al., 2012). Johnson et al. (2012) have recently published a catalog containing 601 ‘confirmed’ clusters (noted as ‘c’) and 237 ‘probable’ candidates (noted as ‘p’). These clusters seem to be less massive than the typical GCs discussed in the current work

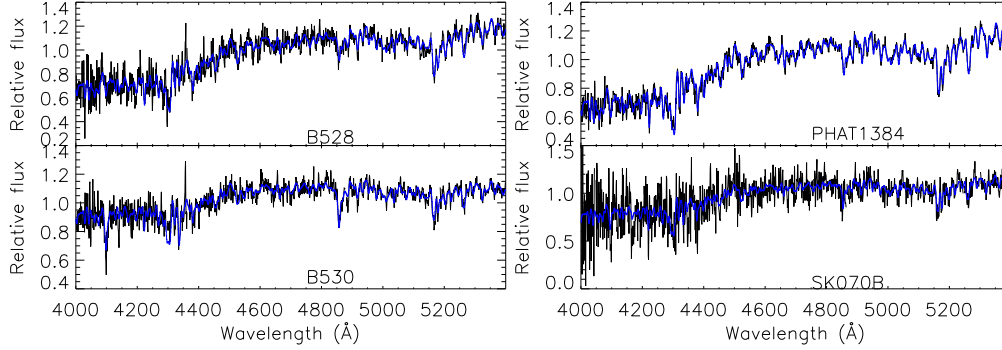


Fig. 10 Same as Fig. 7 but for newly confirmed GCs from the Literature Sample.

Table 4 Updates to classification of objects from the RBC V5 and from Johnson et al. (2012).

Name	RA (deg)	Dec. (deg)	X (kpc)	Y (kpc)	R_p (kpc)	New V_r (km s ⁻¹)	RBC V_r (km s ⁻¹)	Previous classification	New classification
RBC V5									
B530	10.70963	41.42019	1.75	1.05	2.05	-239	99999	2	1
B528	10.79958	41.39664	2.06	0.14	2.07	-197	99999	2	1
SK070B	10.28720	41.16546	-3.57	2.32	4.25	-463	99999	2	1
B233D	10.92214	39.61274	-16.02	-15.64	22.39	99999	99999	2	4
B334D	12.22861	39.59899	-7.73	-26.33	27.44	99999	99999	2	4
B186D	10.00940	39.38665	-24.23	-10.03	26.22	99999	99999	2	4
B412	8.73034	41.54069	-9.05	17.87	20.03	99999	99999	2	4
B504	12.18817	40.14620	-2.28	-21.38	21.50	99999	99999	2	4
SK190B	11.25680	40.40317	-5.55	-11.77	13.01	99999	99999	2	4
SK048C	9.40504	40.09456	-20.46	0.71	20.47	99999	99999	2	4
B411	8.62837	41.56225	-9.43	18.87	21.09	99999	99999	2	4
B339D	12.32291	40.75195	4.91	-17.32	18.01	99999	99999	2	4
B413	8.80411	41.48547	-9.20	16.83	19.18	99999	99999	2	4
SK102B	10.59450	40.37323	-10.06	-6.69	12.07	99999	99999	2	4
WH23	11.25420	41.51660	6.16	-2.46	6.64	-163	-159	6	5
SK026B	9.70296	40.52194	-14.04	1.75	14.15	-491	99999	6	5
SH06	9.82938	40.36611	-14.92	-0.54	14.93	-1047	99999	2	5
PHAT									
PHAT1384	10.67271	41.31956	0.46	0.51	0.69	-284	99999	2	1
PHAT273	11.24446	41.92677	10.42	1.04	10.48	-158	99999	2	5
PHAT1495	11.22254	42.04267	11.51	2.18	11.71	99999	99999	2	5

(Johnson et al., 2012). In our Literature Sample, there are 350 objects from the RBC and 5 objects from Johnson et al. (2012), respectively. Given their closeness to the M31 disk, the SDSS images are not of much help for their identifications. We classify them based on the LAMOST spectra only. Some of the targets have spectra characteristic of, e.g. M-type stars, galaxies and H II regions, and are classified accordingly. If the spectrum has the characteristics of a GC and yields a radial velocity smaller than -150 km s^{-1} , the object is classified as a bona fide GC

296 objects with an original RBC class of 1 or 8 are classified as genuine clusters. These objects are listed in Table 6. The radial velocities newly derived from our spectra, as well as original values from the RBC are listed in the Table. The spectra are all consistent of being GCs. The radial velocities ranging between -726 and 39 km s^{-1} , which are inside the radial velocity range for possible M31 objects. The radial velocities are in good agreement with those from the RBC, with an average difference and scatter of $V_r - V_{r,\text{RBC}} = -11 \pm 22 \text{ km s}^{-1}$. 38 objects are classified as GC candidates in the RBC (class 2).

Table 5 Summary of the catalogs.

	Type	Number
SDSS sample (Tables 2 and 3)	New bona fide GCs	5
	New candidate GCs	23
	Background galaxies	218
	Foreground stars	22
	Quasars	8
	Unknown objects	277
Literature sample (Tables 3, 4 and 5)	Newly confirmed GCs	4
	Previous known GCs	298
	GC candidates	26
	H II regions	11
	Galaxies	16

We find that 3 have radial velocities $V_r < -150 \text{ km s}^{-1}$. They are classified as genuine GCs (class 1) in the current work. 11 candidates have large red-shifts and they are classified as background galaxies (class 4). One target shows strong narrow emission lines classic for H II regions (see the third example spectrum in Fig. 4). Its classification is modified to H II regions (class 5). The remaining candidates have radial velocities $V_r > -150 \text{ km s}^{-1}$ and show no obvious spectral features to help classify them. They could be GCs or foreground MW stars. We retain their classifications as candidate GCs (class 2). Morphological information could be quite helpful for more secure classifications. Two objects originally classified as stars in the RBC (class 6) show spectral features of H II regions and they are reclassified accordingly (class 5). LAMOST spectra of the newly confirmed GCs from the Literature Sample are plotted in Fig. 10 and updates to the classifications of objects from the RBC V5 are listed in Table 4. The newly derived radial velocities (for background galaxies, their radial velocities are noted as “99999”), their original values from the RBC, and the new classifications are listed in the Table.

In Table 4 we also list 3 targets from Johnson et al. (2012) classified by them as possible clusters. We find that one of them (PHAT1384) has a radial velocity of -284 km s^{-1} , and is reclassified as bona fide cluster in the current work. The LAMOST spectrum of PHAT1384 is plotted in Fig. 10. The remaining two candidates show spectral features characteristic of H II regions and are reclassified accordingly. Two objects from Johnson et al. (2012), classified as clusters by them, have spectra compatible of being GCs and have radial velocities of -81 (PHAT224) and -119 km s^{-1} (PHAT1148). These two objects are listed in Table 6 as known clusters.

6 SUMMARY

We present a catalog of 908 targets observed as M31 GC candidates with LAMOST from September, 2011 to June, 2014. A summary of the catalog is presented in Table 5. We have searched for distant clusters amongst targets selected from the SDSS photometry of non-stellar objects in the outer halos of M31 and M33. By combining information from the LAMOST spectra and morphological information from the SDSS images, we identified 5 bona fide GCs and 23 candidates, amongst them 25 are newly discoveries. One of the confirmed GC, LAMOST-2, falls in the halo of M33. Its radial velocity is compatible for being a M33 GC. The other newly discovered bona fide GC (LAMOST-1) falls on the Giant Stream with a projected distance of 78 kpc from M31. The newly identified GC candidates have a maximum projected distance of 265 kpc (LAMOST-C17) from M31. In addition, 218 background galaxies, 8 quasars, 1 white-dwarf-and-main-sequence-star binary, and 21 stars are identified amongst our targets. There are 277 objects exhibiting ambiguous radial velocities and spectral types and cannot be reliably classified as either M31 GCs or foreground MW stars. Images of better resolution than available from the SDSS may help classify these objects.

We have also observed some known GCs and GC candidates selected from the literature. Lists of these objects are provided, including 298 previously known GCs and 32 candidates, containing newly derived radial velocities and updates to the classifications. We have also identified 4 candidates as bona fide M31 GCs based on the newly deduced radial velocities. The LAMOST observations of GCs and

GC candidates provide us a great opportunity to study the GC system of M31. In the current work, 307 confirmed GCs observed by LAMOST are cataloged. The observations, combined with photometric data, yield information of the kinematics, chemistry and age. A full analysis of this data set will be presented in a separate paper.

Acknowledgements We thank the referee for helpful comments and suggestions. This work is partially supported by National Key Basic Research Program of China 2014CB845700 and China Postdoctoral Science Foundation 2014M560843.

This work has made use of data products from the Guoshoujing Telescope (the Large Sky Area Multi-Object Fibre Spectroscopic Telescope, LAMOST). LAMOST is a National Major Scientific Project built by the Chinese Academy of Sciences. Funding for the project has been provided by the National Development and Reform Commission. LAMOST is operated and managed by the National Astronomical Observatories, Chinese Academy of Sciences.

Funding for SDSS-III has been provided by the Alfred P. Sloan Foundation, the Participating Institutions, the National Science Foundation, and the U.S. Department of Energy Office of Science. The SDSS-III web site is <http://www.sdss3.org/>.

SDSS-III is managed by the Astrophysical Research Consortium for the Participating Institutions of the SDSS-III Collaboration including the University of Arizona, the Brazilian Participation Group, Brookhaven National Laboratory, Carnegie Mellon University, University of Florida, the French Participation Group, the German Participation Group, Harvard University, the Instituto de Astrofísica de Canarias, the Michigan State/Notre Dame/JINA Participation Group, Johns Hopkins University, Lawrence Berkeley National Laboratory, Max Planck Institute for Astrophysics, Max Planck Institute for Extraterrestrial Physics, New Mexico State University, New York University, Ohio State University, Pennsylvania State University, University of Portsmouth, Princeton University, the Spanish Participation Group, University of Tokyo, University of Utah, Vanderbilt University, University of Virginia, University of Washington, and Yale University.

References

- Abazajian, K., Adelman-McCarthy, J. K., Agüeros, M. A., et al. 2003, *AJ*, 126, 2081
 Aihara, H., Allende Prieto, C., An, D., et al. 2011, *ApJS*, 193, 29
 Ashman, K. M., & Bird, C. M. 1993, *AJ*, 106, 2281
 Barmby, P., & Huchra, J. P. 2001, *AJ*, 122, 2458
 Barmby, P., Huchra, J. P., Brodie, J. P., et al. 2000, *AJ*, 119, 727
 Battistini, P., Bonoli, F., Braccisi, A., et al. 1987, *A&AS*, 67, 447
 Brodie, J. P., & Huchra, J. P. 1991, *ApJ*, 379, 157
 Brodie, J. P., & Strader, J. 2006, *ARA&A*, 44, 193
 Caldwell, N., Harding, P., Morrison, H., et al. 2009, *AJ*, 137, 94
 Caldwell, N., Schiavon, R., Morrison, H., Rose, J. A., & Harding, P. 2011, *AJ*, 141, 61
 Carignan, C., Chemin, L., Huchtmeier, W. K., & Lockman, F. J. 2006, *ApJ*, 641, L109
 Crampton, D., Cowley, A. P., Schade, D., & Chayer, P. 1985, *ApJ*, 288, 494
 Cui, X.-Q., Zhao, Y.-H., Chu, Y.-Q., et al. 2012, *Research in Astronomy and Astrophysics*, 12, 1197
 de Vaucouleurs, G., de Vaucouleurs, A., Corwin, H. G., Jr., et al. 1991, *Third Reference Catalogue of Bright Galaxies. Volume I: Explanations and references. Volume II: Data for galaxies between 0^h and 12^h. Volume III: Data for galaxies between 12^h and 24^h.*
 di Tullio Zinn, G., & Zinn, R. 2013, *AJ*, 145, 50
 di Tullio Zinn, G., & Zinn, R. 2014, *AJ*, 147, 90
 Drout, M. R., Massey, P., Meynet, G., Tokarz, S., & Caldwell, N. 2009, *ApJ*, 703, 441
 Falcón-Barroso, J., Sánchez-Blázquez, P., Vazdekis, A., et al. 2011, *A&A*, 532, A95
 Fan, Z., Ma, J., de Grijs, R., & Zhou, X. 2008, *MNRAS*, 385, 1973
 Galletti, S., Bellazzini, M., Federici, L., Buzzoni, A., & Fusi Pecci, F. 2007, *A&A*, 471, 127
 Galletti, S., Federici, L., Bellazzini, M., Buzzoni, A., & Fusi Pecci, F. 2006, *A&A*, 456, 985

Table 6 Known GCs from the RBC V5 and from Johnson et al. (2012) observed by LAMOST.

Name	RA (deg)	Dec. (deg)	R_p (kpc)	New V_r (km s ⁻¹)	RBC V_r (km s ⁻¹)	Name	RA (deg)	Dec. (deg)	R_p (kpc)	New V_r (km s ⁻¹)	RBC V_r (km s ⁻¹)
NB21	10.65825	41.26636	0.85	-350	-773	B131	10.71167	41.28542	0.50	-328	-424
B124	10.67261	41.25663	0.21	-255	70	B358	10.82438	39.82032	60.10	-315	-315
B167	10.83802	41.23563	6.69	-368	-231	B338	10.24530	40.59659	13.36	-277	-274
B115	10.64337	41.23387	0.65	-467	-549	B086	10.57773	41.23389	2.70	-272	-189
B225	11.12316	41.35993	12.68	-169	-165	B148	10.76607	41.30136	1.90	-299	-290
B405	12.41585	41.59160	50.66	-170	-162	VDB0	10.12250	40.60414	11.41	-594	-567
B019	10.21887	41.31483	18.34	-232	-224	B012	10.13525	41.36226	23.01	-367	-363
B240	11.35437	41.10616	29.78	-63	-56	B119	10.65043	41.29322	2.09	-316	-310
B106	10.62934	41.20513	1.10	-252	-102	BH05	10.12714	40.75814	8.96	-600	-570
B178	10.87825	41.35459	4.26	-164	-138	MCGC8	13.60396	39.71554	161.44	-380	-381
B127	10.68541	41.24484	0.96	-417	-470	B152	10.79167	41.30447	2.70	-185	-129
B384	11.59138	40.28322	68.85	-366	-364	B058	10.47083	40.78602	12.02	-225	-224
B028	10.31871	40.98422	5.88	-449	-434	B114	10.64292	41.21247	1.05	-374	-271
B077	10.54640	41.12612	2.40	-518	-681	B103	10.62390	41.29928	3.26	-365	-334
B218	11.05968	41.32206	11.66	-225	-220	B027	10.31055	40.93081	5.98	-302	-264
B020	10.23026	41.69037	31.54	-358	-351	B110	10.63793	41.05787	6.62	-244	-247
B123	10.66941	41.17595	3.09	-385	-368	B312	9.91738	40.95068	17.65	-188	-174
B144	10.74942	41.26829	2.36	-352	-140	B158	10.80996	41.12253	9.87	-193	-187
B125	10.67612	41.09197	6.51	-607	-641	B344	10.51239	41.86726	28.53	-256	-252
B179	10.87960	41.30407	5.83	-171	-139	B112	10.63853	41.29511	2.58	-303	-237
B472	10.95173	41.44809	4.55	-126	-106	B163	10.82346	41.46252	3.66	-173	-174
B143	10.74850	41.32206	1.01	-182	-128	B205	10.99239	41.41065	6.60	-374	-373
B171	10.85665	41.26032	6.48	-214	-273	B230	11.14660	40.95342	28.01	-586	-597
B213	11.01463	41.51075	5.36	-461	-545	B099	10.61495	41.16747	1.97	-334	-200
B206	10.99424	41.50502	4.95	-193	-192	B107	10.63022	41.32748	4.08	-319	-337
B311	9.89052	40.52075	12.93	-526	-469	G002	8.39076	39.52187	38.43	-357	-313
B073	10.53048	40.98925	6.21	-505	-481	B324	10.08529	41.68036	36.26	-254	-299
B212	11.01281	41.08231	18.50	-406	-402	B343	10.42958	40.20623	32.56	-361	-360
B064	10.50799	41.18541	3.75	-351	-307	B187	10.91093	41.49634	3.83	-109	-130
B101	10.62093	41.13767	3.14	-401	-489	B403	12.32344	41.58564	47.62	-276	-358
B059	10.47539	41.18354	4.81	-346	-332	B153	10.79421	41.24760	4.69	-262	-231
B063	10.50360	41.48602	14.41	-311	-302	B085	10.57599	40.66588	19.63	-433	-526
B005	10.08462	40.73287	9.58	-299	-265	B017	10.20303	41.20197	15.08	-544	-514
B344D	12.46693	41.61080	51.81	-168	21	B193	10.93962	41.61601	6.48	-79	-59
EXT8	13.31045	41.55686	83.14	-214	-154	B006	10.11031	41.45740	27.28	-244	-237
B386	11.61255	42.03132	14.46	-403	-383	B088	10.58777	41.53729	13.46	-512	-478
B357	10.80513	40.18236	45.59	-348	-285	B190	10.93074	41.56832	5.25	-119	-86
B289	8.58700	41.79753	94.00	-174	-181	B345	10.55888	40.29345	33.28	-361	-293
G327	11.70622	42.74636	29.10	-285	-251	B081	10.55664	40.81083	13.53	-411	-430
B361	10.98787	40.23375	49.79	-353	-330	B034	10.36715	40.89714	6.38	-552	-539
B076	10.54264	41.08946	3.20	-533	-520	B105	10.62810	41.50759	10.98	-264	-238
B302	9.63964	41.34790	40.39	-428	-371	B381	11.52728	41.34969	27.40	-78	-86
B066	10.51287	40.74642	14.67	-438	-389	B234	11.19334	41.48827	11.27	-204	-207
B350	10.61847	40.41423	30.58	-430	-467	B400	12.00599	42.42583	20.63	-262	-258
B292	9.06941	40.97404	48.75	-374	-307	B201	10.97016	41.16611	13.92	-725	-706
B397	11.86348	41.20290	44.48	-125	-228	B373	11.42436	41.75929	12.55	-229	-219
B233	11.17549	41.73180	7.94	-79	-74	B383	11.54978	41.32822	28.93	-234	-253
B156	10.80719	41.02159	13.59	-384	-400	MGC1	12.67691	32.91633	391.24	-355	-355
B039	10.40779	41.34716	12.69	-253	-243	B130	10.70356	41.49794	8.15	-53	-25
B223	11.11271	41.57699	6.99	-74	-101	B174	10.87623	41.64896	8.91	-489	-478
B161	10.81421	41.19027	7.49	-436	-413	B082	10.56601	41.02063	5.97	-383	-366
B065	10.50807	40.67026	17.40	-404	-382	B339	10.25296	39.93169	37.59	-242	-188
B293	9.08691	40.89363	45.60	-526	-424	SK007A	9.93363	40.85526	14.72	-446	-390
B317	9.98030	41.79614	44.20	-202	-143	B060	10.48750	41.08735	3.17	-537	-484
B098	10.61408	40.99333	8.35	-314	-268	B094	10.60434	40.95489	9.51	-564	-565
B091	10.59046	41.36817	6.98	-302	-290	B188	10.92297	41.40721	4.45	-185	-184
B365	11.15185	42.28902	25.28	-76	-67	B025	10.30230	41.00781	6.51	-249	-206
B313	9.93587	40.88195	15.26	-439	-440	B352	10.65911	42.03696	30.20	-298	-164
B204	10.98510	41.36747	7.57	-340	-352	B096	10.60863	41.32072	4.58	-319	-260
B157	10.80821	41.18880	7.33	-266	4	B180	10.88221	41.12952	12.14	-213	-202
B038	10.39983	41.32077	12.04	-191	-175	B042	10.42367	41.12394	5.04	-313	-338
V014	10.30755	40.56607	15.77	-467	-450	B080	10.55160	41.31685	6.47	-298	-255
B087D	10.74546	41.15242	6.51	-452	-661	B315	9.95223	40.52513	12.51	-560	-437
B399	11.99811	41.59126	36.05	-426	-437	B401	12.03546	41.67830	34.60	-352	-333
B134	10.71522	41.23433	2.37	-274	-369	B291	9.02071	42.03592	86.83	-220	-215
B323	10.07620	40.54580	12.43	-525	-500	B001	9.96253	40.96963	16.60	-222	-179
B306	9.78627	40.57250	14.58	-440	-424	G260	11.00352	42.58008	40.40	-213	16
B407	12.54149	41.68366	52.01	-315	-338	B020D	10.32182	41.13588	8.78	-479	-526
B194	10.93828	41.10239	15.12	-401	-354	B141	10.74703	41.54651	8.66	-187	-180

Table 6 Continued.

Name	RA (deg)	Dec. (deg)	R_p (kpc)	New V_r (km s ⁻¹)	RBC V_r (km s ⁻¹)	Name	RA (deg)	Dec. (deg)	R_p (kpc)	New V_r (km s ⁻¹)	RBC V_r (km s ⁻¹)
B235	11.24136	41.48998	12.85	-97	-98	B051	10.44454	41.42199	14.10	-258	-270
B486	11.53571	40.96769	41.28	-204	-152	B202	10.97784	41.00895	20.00	-246	-343
B257	10.51371	40.97052	6.48	-486	-476	B004	10.07462	41.37787	25.74	-381	-369
B337	10.20202	42.20304	51.68	-294	50	B135	10.71653	41.51895	8.55	-372	-371
B217	11.04416	41.39752	8.73	-52	-25	B189	10.92663	41.58984	5.89	-143	-148
B176	10.87690	40.81964	23.65	-536	-521	B310	9.85724	41.39256	34.08	-256	-206
B319	10.01279	40.56620	11.78	-565	-535	B370	11.31000	41.96132	11.77	-374	-352
B150D	9.24949	41.42505	57.16	-269	99999	B382	11.54312	41.62790	19.21	-272	-302
B216	11.03659	41.63217	6.11	-80	-93	B256D	11.24469	41.91020	11.01	-86	-74
G085	10.30333	40.57144	15.48	-468	-444	B031	10.33716	40.98449	5.52	-377	-400
B008	10.12613	41.26907	20.11	-330	-319	B255	10.50003	40.80945	11.95	-438	-433
B097	10.61443	41.42560	8.32	-290	-283	B083	10.56852	41.75572	22.42	-391	-347
B185	10.90534	41.24543	8.75	-198	-163	B036	10.38677	41.43478	16.62	-510	-341
B314	9.93581	40.23553	19.14	-490	-485	B018	10.20583	40.69220	9.98	-593	-585
B393	11.75501	41.40185	33.72	-395	-331	NB89	10.68658	41.24561	0.97	-280	-332
B391	11.74205	41.56579	27.91	-320	-325	B049	10.43987	40.83194	9.59	-478	-481
B325	10.09632	40.51310	13.47	-636	-560	B147	10.76375	41.35604	1.47	-216	-51
B322	10.07186	40.65123	10.40	-594	-581	B029	10.32433	41.00640	5.93	-516	-374
B111	10.63826	41.00732	8.55	-444	-414	B022	10.24616	41.41172	20.79	-463	-407
B003	10.03917	41.18478	20.42	-381	-351	H19	11.06200	38.42839	121.52	-285	99999
B011	10.13282	41.65474	33.64	-249	-178	B295	9.19471	40.32842	27.21	-418	-408
B448	10.15211	40.67088	10.10	-554	-552	G268	11.04174	42.78273	47.01	-296	-321
B214	11.01641	41.43850	6.69	-183	-258	B301	9.58998	40.06029	20.26	-389	-382
B349	10.60053	40.62886	21.81	-407	-406	B222	11.10563	41.23665	16.23	-324	-303
SK104A	11.43463	41.95772	11.96	-172	-301	B016	10.18821	41.36939	21.36	-389	-406
B347	10.59537	41.90760	27.32	-283	-251	B304	9.73726	41.17456	31.00	-414	-341
H26	14.86404	37.69281	284.25	-419	99999	B380	11.52583	42.01472	13.23	-111	-13
MCGC10	16.85966	35.78011	430.68	-300	-291	B033	10.35999	41.00382	5.15	-455	-439
B457	10.37170	42.31032	50.04	-333	-63	B015	10.18757	40.99893	9.78	-467	-460
B236	11.28712	40.84132	37.14	-410	-411	B172	10.85832	41.35884	3.49	-187	-272
H17	10.59870	37.24308	151.04	-233	99999	B129	10.70135	41.41852	5.18	-109	-75
B013	10.16022	41.42328	24.28	-422	-409	B372	11.38908	42.00678	12.43	-226	-216
V031	10.30100	41.09133	8.28	-480	-433	B010	10.13154	41.23956	18.91	-195	-161
B196	10.95239	40.71025	30.40	-330	-313	M086	11.36870	41.82488	10.71	-56	-32
B287	11.36873	41.50128	16.90	-226	-281	B477	11.28471	41.66053	10.31	-123	-110
B106D	10.97687	41.25381	11.02	-282	-312	B116	10.64390	41.54760	11.98	-357	-337
B290	8.58725	41.47169	82.80	-439	-381	B122	10.66703	41.56299	11.81	-415	-437
B061	10.50050	41.49328	14.79	-284	-285	B376	11.45161	41.71108	14.20	-125	-163
B045	10.42962	41.57222	20.20	-415	-425	B047	10.43982	41.70107	24.69	-299	-291
B228	11.13842	41.69107	7.29	-435	-457	B229	11.14085	41.64127	7.16	-58	-31
B387	11.63959	40.73711	53.49	39	-297	G353	12.57577	42.59559	30.39	-297	-295
B182	10.90280	41.13670	12.60	-350	-347	MCGC9	13.93309	42.77114	66.06	-131	-147
B422	9.41034	41.99995	71.71	-212	-202	B316	9.99329	40.69416	11.38	-388	-348
B220	11.08102	41.50969	7.15	-241	-247	B048	10.43965	41.22517	7.34	-359	-251
B337D	12.29681	41.12245	62.74	-285	-222	B002	10.01072	41.19822	21.89	-370	-338
SK086A	11.10863	41.58734	6.80	-76	-69	B402	12.15023	42.02624	28.73	-420	-488
B467	10.77679	42.03033	26.23	-294	-342	B160	10.81224	41.02652	13.57	-383	-354
B177	10.87713	41.09509	13.24	-385	-403	B211	11.01214	41.33464	9.55	-211	-60
B367	11.19654	42.09218	17.19	-66	-152	H7	7.97715	40.11312	63.17	-446	99999
B183	10.90391	41.03398	16.47	-203	-186	B378	11.48848	41.89188	12.68	-224	-205
B375	11.43983	41.66175	14.94	-196	-209	B024	10.29938	41.76369	31.87	-232	-310
B307	9.82689	40.54948	13.68	-477	-397	B115D	11.11090	41.64960	6.74	-111	99999
B074	10.53354	41.72269	22.33	-463	-435	B336	10.19837	42.14503	49.62	-651	-609
B151	10.78976	41.35892	1.66	-202	-330	B305	9.74522	40.27559	16.62	-436	-489
B056	10.46316	40.96114	5.78	-32	-382	B032	10.33965	41.29170	13.19	-534	-516
B186	10.90923	41.60681	6.72	-144	-119	B303	9.71053	40.45860	15.58	-500	-464
V133	11.29390	42.00333	12.89	-466	-58	B046	10.43593	41.77450	27.59	-370	-98
B051D	10.58568	41.07724	4.43	-31	-209	B468	10.80228	39.79926	60.17	-279	-278
SK053A	10.67003	40.29801	36.69	-408	-348	H20	11.46881	39.93116	77.96	-75	99999
B461	10.51773	42.05738	35.59	-307	-296	B075	10.53681	41.33923	7.81	-146	-212
B351	10.65821	42.19192	36.16	-320	-325	B354	10.69835	42.00712	27.81	-186	-283
B396	11.85482	40.36168	75.16	-644	-561	SK073A	10.95221	41.13006	14.60	-413	-33
H16	10.15756	39.75831	41.26	-410	99999	B093	10.59644	41.36207	6.55	-298	-447
B423	9.48630	40.95987	33.22	-270	-215	B309	9.85262	40.24141	17.89	-417	-480
B266	10.76465	41.67541	13.04	-191	-161	B462	10.56134	42.02681	32.99	-250	-214
B237	11.28852	41.37624	18.02	-102	-86	B078	10.55063	41.29967	5.88	-333	-260
B072	10.53087	41.37990	9.51	-142	-89	B041D	10.51969	41.27972	6.29	-372	-289
B398	11.99074	41.81264	29.10	-197	-227	B023	10.25494	41.22938	14.12	-343	-451
B260	10.63829	41.52351	11.25	-189	-190	B209	11.01097	41.42406	6.87	-328	-460
B165	10.82590	41.18186	8.22	-191	-35	B095	10.60748	41.09343	4.40	-155	-233

Table 6 Continued.

Name	RA (deg)	Dec. (deg)	R_p (kpc)	New V_r (km s ⁻¹)	RBC V_r (km s ⁻¹)	Name	RA (deg)	Dec. (deg)	R_p (kpc)	New V_r (km s ⁻¹)	RBC V_r (km s ⁻¹)
B068	10.51336	40.98062	6.12	-310	-278	B109	10.63401	41.17442	2.15	-571	-372
B232	11.16762	41.25012	17.98	-183	-182	B011D	10.21508	40.73504	9.05	-538	-481
KHM31-74	10.22055	40.58880	13.14	-55	-576	B035	10.38578	41.64238	24.34	-45	-49
B342	10.35046	40.61310	15.16	-350	-479	B075	10.53668	41.33922	7.81	-246	-212
B298	9.50106	40.73223	26.17	141	-539	B037	10.39570	41.24859	9.69	-304	-338
B283	11.23083	41.28332	19.09	-69	-83	B199	10.95759	40.97071	20.72	-415	-396
B168	10.84385	41.73489	12.97	-139	-190	B341	10.28813	40.59805	14.21	-2	-321
PHAT	11.24690	41.91080	11.00	-81	99999	PHAT	11.12700	41.84364	10.47	-119	99999

- Galletti, S., Federici, L., Bellazzini, M., Fusi Pecci, F., & Macrina, S. 2004, *A&A*, 416, 917
- Harris, W. E. 1996, *AJ*, 112, 1487
- Hubble, E. 1932, *ApJ*, 76, 44
- Huchra, J. P., Brodie, J. P., & Kent, S. M. 1991, *ApJ*, 370, 495
- Huo, Z.-Y., Liu, X.-W., Xiang, M.-S., et al. 2013, *AJ*, 145, 159
- Huo, Z.-Y., Liu, X.-W., Yuan, H.-B., et al. 2010, *Research in Astronomy and Astrophysics*, 10, 612
- Huxor, A. P., Mackey, A. D., Ferguson, A. M. N., et al. 2014, *MNRAS*, 442, 2165
- Huxor, A. P., Tanvir, N. R., Ferguson, A. M. N., et al. 2008, *MNRAS*, 385, 1989
- Ibata, R. A., Lewis, G. F., McConnachie, A. W., et al. 2014, *ApJ*, 780, 128
- Johnson, L. C., Seth, A. C., Dalcanton, J. J., et al. 2012, *ApJ*, 752, 95
- Kent, S. M. 1989, *PASP*, 101, 489
- Kim, S. C., Lee, M. G., Geisler, D., et al. 2007, *AJ*, 134, 706
- Koleva, M., Prugniel, P., Bouchard, A., & Wu, Y. 2009, *A&A*, 501, 1269
- Lee, M. G., Hwang, H. S., Kim, S. C., et al. 2008, *ApJ*, 674, 886
- Liu, X.-W., Yuan, H.-B., Huo, Z.-Y., et al. 2014, in *IAU Symposium*, *IAU Symposium*, vol. 298, edited by S. Feltzing, G. Zhao, N. A. Walton, & P. Whitelock, 310–321
- Luo A.-L., et al. 2015, *RAA*, in press
- Lupton, R., & Ivezić, Ž. 2005, in *Astrometry in the Age of the Next Generation of Large Telescopes*, *Astronomical Society of the Pacific Conference Series*, vol. 338, edited by P. K. Seidelmann & A. K. B. Monet, 151
- Ma, J., Wang, S., Wu, Z., et al. 2015, *AJ*, 149, 56
- Mackey, A. D., Huxor, A. P., Ferguson, A. M. N., et al. 2013, *MNRAS*, 429, 281
- McConnachie, A. W. 2012, *AJ*, 144, 4
- Peacock, M. B., Maccarone, T. J., Knigge, C., et al. 2010, *MNRAS*, 402, 803
- Perrett, K. M., Bridges, T. J., Hanes, D. A., et al. 2002, *AJ*, 123, 2490
- Prugniel, P., & Soubiran, C. 2001, *A&A*, 369, 1048
- Prugniel, P., Soubiran, C., Koleva, M., & Le Borgne, D. 2007, *ArXiv Astrophysics e-prints*
- Renzini, A., & Fusi Pecci, F. 1988, *ARA&A*, 26, 199
- Richardson, J. C., Irwin, M. J., McConnachie, A. W., et al. 2011, *ApJ*, 732, 76
- Robin, A. C., Reyl  , C., Derri  re, S., & Picaud, S. 2003, *A&A*, 409, 523
- Rubin, V. C., & Ford, W. K., Jr. 1970, *ApJ*, 159, 379
- Sakari, C. M., Venn, K. A., Mackey, D., et al. 2015, *ArXiv e-prints*
- S  nchez-Bl  zquez, P., Peletier, R. F., Jim  nez-Vicente, J., et al. 2006, *MNRAS*, 371, 703
- Sargent, W. L. W., Kowal, C. T., Hartwick, F. D. A., & van den Bergh, S. 1977, *AJ*, 82, 947
- Schlafly, E. F., Green, G., Finkbeiner, D. P., et al. 2014, *ApJ*, 786, 29
- Tanvir, N. R., Mackey, A. D., Ferguson, A. M. N., et al. 2012, *MNRAS*, 422, 162
- van den Bergh, S. 1969, *ApJS*, 19, 145
- Vazdekis, A., S  nchez-Bl  zquez, P., Falc  n-Barroso, J., et al. 2010, *MNRAS*, 404, 1639
- Veljanoski, J., Mackey, A. D., Ferguson, A. M. N., et al. 2014, *MNRAS*, 442, 2929

- Xiang, M. S., Liu, X. W., Yuan, H. B., et al. 2015a, MNRAS, 448, 90
- Xiang, M. S., Liu, X. W., Yuan, H. B., et al. 2015b, MNRAS, 448, 822
- York, D. G., Adelman, J., Anderson, J. E., Jr., et al. 2000, AJ, 120, 1579
- Yuan, H.-B. 2013, in IAU Symposium, *IAU Symposium*, vol. 295, edited by D. Thomas, A. Pasquali, & I. Ferreras, 239–239
- Yuan, H.-B., Liu, X.-W., Huo, Z.-Y., et al. 2010, Research in Astronomy and Astrophysics, 10, 599
- Yuan, H.-B., Liu, X.-W., Huo, Z.-Y., et al. 2015, MNRAS, 448, 855